

pubs.acs.org/JPCA Article

Chemical Activation of Water Molecule by Collision with Spin-Orbit-State-Selected Vanadium Cation: Quantum-Electronic-State Control of Chemical Reactivity

Published as part of The Journal of Physical Chemistry virtual special issue "Cheuk-Yiu Ng Festschrift". Yuntao Xu, Yih-Chung Chang, Matthew Parziale, Anna Wannenmacher, and Cheuk-Yiu Ng*



Cite This: J. Phys. Chem. A 2020, 124, 8884–8896

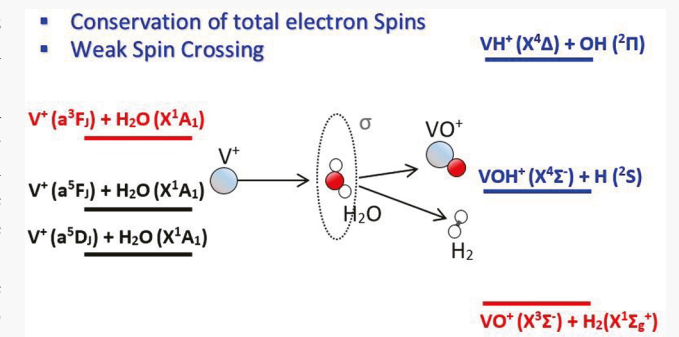


ACCESS

Metrics & More

Article Recommendations

ABSTRACT: We have obtained absolute integral cross sections $(\sigma's)$ for the reactions of spin—orbit-state-selected vanadium cations, V⁺[$a^5D_J(J=0,2)$, $a^5F_J(J=1,2)$, and $a^3F_J(J=2,3)$], with a water molecule (H_2O) in the center-of-mass collision energy range $E_{cm}=0.1-10.0$ eV. On the basis of these state-selected σ curves $(\sigma$ versus E_{cm} plots) observed, three reaction product channels, VO⁺ + H₂, VH⁺ + OH, and VOH⁺ + H, from the V⁺ + H₂O reaction are unambiguously identified. Contrary to the previous guided ion beam study of the V⁺(a^5D_J) + D₂O reaction, we have observed the formation of the VO⁺ + H₂ channel from the V⁺(a^5D_J) + H₂O ground reactant state at low E_{cm} 's (<3.0 eV). No spin—orbit J-state dependences for the σ curves of individual



electronic states are discernible, indicating that spin—orbit interactions are weak with little effect on chemical reactivity of the titled reaction. For the three product channels identified, the triplet $\sigma(a^3F_J)$ values are overwhelmingly higher than the quintet $\sigma(a^5D_J)$ and $\sigma(a^5F_J)$ values, showing that the reaction is governed by a "weak quintet—triplet spin crossing" mechanism, favoring the conservation of total electron spins. The σ curves for exothermic product channels are found to exhibit a rapid decreasing profile as E_{cm} is increased, an observation consistent with the prediction of the charge—dipole and induced-dipole orbiting model. This experiment shows that the V⁺ + H₂O reaction can be controlled effectively to produce predominantly the VO⁺ + H₂ channel via the V⁺(a³F_J) + H₂O reaction at low E_{cm} 's (\leq 0.1 eV) and that the ion—molecule reaction dynamics can be altered readily by selecting the electronic state of V⁺ cation. On the basis of the measured E_{cm} thresholds for the $\sigma(a^5D_J)$ a⁵F_J and a³F_J: VH⁺) and $\sigma(a^5D_J)$ a⁵F_J, and a³F_J: VOH⁺) curves, we have deduced upper bound values of 2.6 \pm 0.2 and 4.3 \pm 0.3 eV for the 0 K bond dissociation energies, $D_0(V^+-H)$ and $D_0(V^+-OH)$, respectively. After correcting for the kinetic energy distribution resulting from the Doppler broadening effect of the H₂O molecule, we obtain $D_0(V^+-H) = 2.2 \pm 0.2$ eV and $D_0(V^+-OH) = 4.0 \pm 0.3$ eV, which are in agreement with D_0 determinations obtained by σ curve simulations.

I. INTRODUCTION

The fundamental investigation of chemical reactivity or absolute integral reaction cross sections (σ 's) for the reactions between transition metal (TM) cations and water molecule (H_2O) is important for many research fields that are of energy and environmental relevance, such as catalytic chemistry^{1,2} and water splitting.³ The complex electronic structures of TM cations resulting from interactions of valence electrons residing in partially filled d- or f-electronic subshells and the demanding experimental techniques required for chemical reactivity measurements have made both theoretical and experimental studies on chemical reactivity of TM cations highly challenging. To our best knowledge, quantum-electronic-state-resolved ion–molecule reactions study involving TM cations with the H_2O molecule have not yet been achieved.

The low-lying electronic states along with a variety of electron spin multiplicities^{4,5} for TM cations are believed to be responsible for their versatile bonding abilities. According to the forbidden nature of the parity and electron spin selection rules, $^{6-8}$ these low-lying electronic states of TM cations are expected to be long-lived with radiative lifetimes significantly longer than the experimental cycles. This expectation has been confirmed in recent chemical reactivity studies of the V⁺(a⁵D₁)

Received: August 29, 2020 Revised: October 9, 2020 Published: October 20, 2020





 a^5F_J , and a^3F_J) + D₂ (CO₂, CH₄) reactions. ^{9,10} The characteristics of low-lying in energy and long lifetimes make it mandatory to account for the chemical reactivity of individual electronic states for any realistic investigations of the bonding and catalytic properties of TM cations. Hence, the capability for performing quantitative chemical reactivity measurements as a function of low-lying electronic state represents a key experimental development, which is expected to provide valuable mechanistic understanding on the chemical reactivity of TM cations. ^{11–14}

The primary goal of quantum-state-selected ion-molecule reaction studies is to answer a central question in chemistry, which is concerned with understanding the roles that the different modes of quantum states play in promoting or suppressing chemical reactivity. 14-20 In past decades, many efforts have been devoted to understanding the internal vibrational effects on chemical reactivity. 21-24 However, the general investigations on quantum rotational and electronicstate effects have been relatively unexplored. According to the Born-Oppenheimer approximation, the molecular geometry is mostly governed by the electron arrangement of the molecule. Thus, we expect that by changing the quantum-electronic state is equivalent to altering the electron arrangement of reactant ion and thus can greatly alter its chemical reactivity. It has been speculated for a long while whether different forms of angular momentum states of TM ion can have different effects on chemical reactivity of ions. $^{11-13}$ The answer to this question requires spin-orbit electronic-state-selected σ measurements for ion-molecule reactions of TM ions, including those of the present study and the most recently reported experiments on the $V^+(a^5D_I, a^5F_I, and a^3F_I) + D_2$ (CO₂, CH₄) reaction systems. 9,10

Theoretical and computation chemistry have made tremendous progress in past decades. However, due to the more complex electronic structures of TM cations, the state-of-theart theoretical energetics and chemical dynamics calculations are known to have larger error limits for chemical reaction systems of TM species than those of main group elements. 25,2 To help with the further theoretical development and thus improve the accuracy of chemical reactivity predictions of ionmolecule reactions of TM cations, accurate experimental σ measurements are needed for the benchmarking efforts. The present spin-orbit electronic-state-selected σ measurements on the V^+ + H_2O reaction, along with the most recently reported σ measurements for the V⁺ + D₂ (CO₂, CH₄) reactions, 9,10 have all been aimed to provide experimental benchmarking cross sections for the further development of more accurate theoretical procedures for reaction dynamics predictions of TM cations.

Numerous mass spectrometric studies of gaseous ion—molecule reactions between TM cations and the $\rm H_2O$ molecule have been reported previously. In particular, the V+ + H₂O reaction, recognized as a model ion—molecule reaction for TM cation, has received the attention of several previous experimental and theoretical investigations. $^{27-29}$ Since chemical reactivity measurements performed in the gas phase represent measurements under mostly idealized conditions, where the σ values are free from interferences by solvents, interfaces, and other impurities, we expect that gaseous σ measurements can provide unbiased insight into the reaction mechanisms.

Previous mass spectrometric studies have also provided information on possible product ion channels of the $V^+ + H_2O$

reaction.³⁰ Furthermore, previous spectroscopic and theoretical studies have yielded insight into the structures of possible ion–molecule intermediates that might be involved in the V⁺ + $\rm H_2O$ reaction.³⁰ Two intermediate structures are proposed: one has a $\rm C_{2\nu}$ symmetry with the V⁺OH₂ ion–molecule complex structure formed by linking the V⁺ ion to the O atom of the $\rm H_2O$ molecule, and the other is the inserted HV⁺OH structure formed by inserting V⁺ ion into an OH bond of the H₂O molecule. The formation of the V⁺OH₂ ion–molecule adduct has been confirmed in a previous flow-tube chemical kinetics study.²⁹

Nearly all previous experimetnal studies on the V++ H2O reaction system were carried out with reactant V+ ions quenched to the ground electronic state by collisions with a carrier gas, such as helium.²⁹ However, as pointed out previously, the distributions of electronic states thus prepared remain uncertain because the collision relaxation mechanisms involved are different for different TM cations. On the basis of the guided ion beam (GIB) mass spctrometric study conducted at different ion source conditions, such as the temperature, Clemmer et al. were able to suggest that reactant V^+ ion prepared in its triplet a^3F_I state is much more reactive toward D_2O compared to the quintet a^5D_1 ground state.²⁷ The chemical kinetics study, which has been reported on the observation of product VO+ at room temperature, 29 was not consistent with the observation of the previous GIB study, in which VO⁺ ions were only observed at $E_{\rm cm} > 3$ eV. Previous σ measurements for the V++ D2O reaction can be ascribed to reactant V⁺ ions prepared mostly in the a⁵D_I ground state, and quantitative chemical reactivity measurements with V⁺ ions prepared in single excited electronic states have not been made. We note that the previous GIB study only reported on the V⁺ + D₂O reaction, ²⁷ and the electronic-state-selected study on the V+ + H2O reaction has not been reported previously.

Recently, a novel two-color visible-ultraviolet (vis-UV) laser pulsed field ionization-photoion (PFI-PI) detection method has been reported and successfully used to prepare V⁺ ions with 100% purity in each of its 13 spin—orbit-coupled *J* states: $a^5D_I(J = 0-4)$, $a^5F_I(J = 1-5)$, and $a^3F_I(J = 2-4)$, where J is the total angular momentum of the coupled electron spin and orbital angular momentum.³¹ By combining this quantumelectonic-state-selected V⁺ ion source with the doublequadruple-double-octopole (DQDO) mass spectrometer developed in our laboratory, we can obtain detailed σ measurements of ion-molecule reactions involving V+ ions with neutral molecules as a function of the low-lying quantumelectronic state of V^+ ion as well as the $E_{\rm cm}$ of the reaction. We have recently reported on detailed spin-orbit-electronic-stateselected σ measurements of the reaction systems of V⁺[a⁵D_I(J = 0, 2), $a^5F_I(J = 1, 2)$, and $a^3F_I(J = 2, 3)$, $+ D_2(CO_2)$ CH₄). 9,10 As an ongoing research effort to investigate chemical reactivity between quantum-electronic-state-selected TM cations and neutral atmospheric molecules, we present in this work detailed σ measurements of the V⁺[a⁵D_I(J = 0, 2), a⁵F_I(J= 1, 2), and $a^3F_I(J=2,3)$] + H₂O reactions. We shows below that by electronic-state selection, these reactions can serve as an efficient source of H₂.

As an important chemical feedstock in refining petroleum and synthesizing fertilizers, H_2 has been produced annually at more than 44.5 million tons. Water splitting is currently a hot research topic, aiming to convert water molecules into H_2 + O_2 at low cost. Since the combustion of H_2 in O_2 regenerates

the H₂O molecule, H₂ is an ideal energy carrier without any environmental problems. Currently, besides water splitting, which only provides about 5% of the H₂ production, there are two other approaches based on steam methane re-forming and coal gasification, which are used to provide more than 95% of the total H₂ production need. Unlike water splitting, both of these methods rely on nonrenewable fossil fuels and generate CO₂ as the byproduct. Therefore, even though water splitting has a relatively higher cost, it still represents one of the future directions to provide clean and renewable energy. Numerous efforts have been made to lower the cost of water splitting by using non-trace-metal catalysts, which are abundant on Earth. Transition metals have been considered among the most promising candidates for this purpose.³⁴ One of the bottlenecks limiting the further development of water splitting with TMs is the lack of understanding of the fundamental reaction mechanism of related chemical processes. The present work has shed some light on the chemical reaction dynamics involved by measuring the chemical reactivity of the V+ ion toward the H2O molecule as a function of the quantumelectronic state and kinetic energy of the V⁺ ion. In particular, valuable insights into the mechanism for achieving efficient control of H₂ production have been gained. We hope that such mechanistic information will make its way into future designs of catalytic cycles used in practical water splitting reactors.

II. EXPERIMENTAL CONSIDERATIONS

The two-color vis—UV laser PFI-PI experimental method for preparing quantum-electronic-state-selected reactant V⁺ ions, the arrangement of the PFI-PI DQDO ion—molecule reaction aparatus, and the procedures employed in using this apparatus for σ measurements have all been described in detail previously; ^{10,31} thus, only a brief description on these aspects is given below.

Ila. Two-Color Vis-UV laser PFI-PI Metal Ion Source. The gaseous precursor sample of neutral V atoms was generated from a metal atom beam source formed by pulsed laser ablation. The second harmonics (532 nm) of a pulsed Nd:YAG laser (pulse energy = 2 mJ, repetition rate = 30 Hz) is employed to ablate a rotating and translating V metal rod. The plumes of the charged and neutral species thus generated are carried forward by a pulsed supersonic He beam traveling along the central axis of the PFI-PI DQDO ion-molecule reaction aparatus. The charged species are removed from the V beam by using a DC electric field, and thus only neutral V species can enter the photoexcitation (PEX) region, which is defined by the region between ion lenses E1 and I1. The three ion lenses E1, I1, and I2 are key elements of the ion source. The V/He seeded beam intersects the vis and UV lasers at the PEX center. The vis and UV laser outputs are generated from two dye lasers pumped by an identical pulsed Nd:YAG laser. The neutral V atom beams are excited first by the vis laser to a fixed neutral intermediate state before further excitation by the UV laser to high-n $(n \ge 60)$ Rydberg states $[V^*(n)]$, which converge to selected ionization limits of V atom of interest. Prompt V⁺ ions without state selections are also formed by direct photoionizations of V atoms as well as by autoionizations of excited V atoms. The long lifetimes of high-n (n \geq 60) Rydberg states allow the application of a small pulsed electric field (magnitude = 2.0 eV and duration = 2.0 μ s) to ion lens I1 to retard the prompt ions from the $V^*(n)$ beam. Thus, the prompt ions can be separated spatially from the $V^*(n)$ beam. At a delay of 10 ns with respect to turning off the first

pulsed electric field, a second pulsed electric field (magnitude = 41.7 eV and duration = 0.75 μ s) is applied to ion lens E1, to pulsed-field ionize the $V^*(n)$ to generate V^+ ions in selected electronic states. The second PFI electric field also serves to extract the PFI-PIs and prompt ions out of the PEX region. It is important to switch off the PFI electric field before the V⁺ PFI-PI ions exit the PEX region, such that all the V+PFI-PIs gain the same kinetic energy from the ion extraction process. The application of this sequential pulsing scheme is the key to achieving high kinetic energy resolution of V⁺ PFI-PIs. Due to the application of the pulsed retarding electric field, the prompt ions have gained a negative momentum, and thus, the final resulting kinetic energy is lower than that of the V+ PFI-PI ions. As a result, a small positive DC voltage can be applied to ion lens I2, serving as an effective potential barrier, to block off prompt ions from staying in the V+ PFI-PI beam. With a sufficiently high PFI-PI resolution achieved in the present experiment, only $V^{\scriptscriptstyle +}$ PFI-PI ions in single-selected spin-orbit electronic states can enter the reaction gas cell to react with neutral H₂O molecules.

Readers are referred to the two-color laser PFI-PI spectra for $V^+[a^5D_J(J=0-4)]$, $V^+[a^5F_J(J=1-5)]$, and $V^+[a^3F_J(J=2-4)]$ shown in Figure 8a–c in ref 31, respectively. The *J*-state assignments are marked below the PFI-PI spectra for individual spin—orbit electronic states. The retarding and PFI electric field pulses (F_R and F_{PFI}) used were given in individual figures. The ionization energy (IE) values for all these spin—orbit states are known and are also given and marked by long dropline shown in these figures. The fully *J*-resolved PFI-PI spectra observed indicate that the preparation of V^+ ion in single quantum spin—orbit electronic states is achieved.

IIb. PFI-PI DQDO Ion-Molecule Reaction Aparatus. The PFI-PI DQDO ion-molecule reaction appratus can be separated into five components. In sequential order, these include the reactant PFI-PI ion source, a reactant quadrupole mass filter (QMF), a radio frequency (rf)-octopole ion guide reaction gas cell, a product QMF, and an ion detecting system.³⁵ The reactant QMF is designed for reactant ion selections. In the present study, this QMF is only used as a focusing ion lens for guiding V+ ions formed in the ion source to enter the rf octopole ion guide reaction gas cell, where reactions between V⁺ PFI-PI and the H₂O molecule occur. The pressure of the reaction gas cell is monitored by a MKS Baratron, and the gas flow is controlled by an electromagnetic valve. The typical pressure of H_2O vapor used for σ measurements is 2.0×10^{-4} Torr. The ion detecting system is composed of a modified Daly type ion detector, in which the photomultiplier-scintilation assembly is replaced by a dual set of microchannel plate (MCP) ion detectors. The data acquisition for σ measurements is controlled by a personal computer.

Ilc. Absolute Integral Cross Section Measurements. As pointed out above, the chemical reactivity can be directly determined by absolute integral cross section (σ) measurements, which are obtained by comparing the intensity of the reactant V^+ ions and that of the product ions. By using the thin target ion-neutral scattering scheme, we can deduce σ as $[(kT)/(Pl)][\ln((I+i)/I)]$, where k, T, P, l, I, and i represent the Boltzmann constant, the temperature in degree K, the pressure of the neutral reactant in the reactant gas cell, the effective length of the gas cell, the intensity of the unreacted reactant V^+ ions, and the intensity of the product ions, respectively. The σ values determined in the present study are

the average of at least three independent measurements. The run-to-run uncertainty is in the range 5–10%. The error limits for absolute σ values are estimated to be about 30%.

The $E_{\rm cm}$ is converted from the laboratory kinetic energy $(E_{\rm lab})$ by using the formula $E_{\rm cm} = E_{\rm lab}[M/(m^+ + M)]$, where m^+ and M are the masses of the V⁺ ion and the neutral molecule H₂O, respectively. As pointed out in previous studies, ³⁶ for an ion beam—gas cell study as in this case, the thermal motions of neutral molecules in the reaction gas cell can be the main contribution to the $E_{\rm cm}$ spread $(\Delta E_{\rm cm})$, especially in the low $E_{\rm cm}$ range. For the reaction of V⁺ + H₂O, the estimated uncertainties for $E_{\rm cm} = 0.1, 0.5, 1.0$, and 4.0 eV are 0.1, 0.3, 0.5, and 0.9 eV, respectively. The $\Delta E_{\rm cm}$ spread can have the effect of smoothing the structures of the $\sigma(E_{\rm cm})$ curves. However, the general trends for the $\sigma(E_{\rm cm})$ curves are not expected to be greatly affected.

Similar to the σ measurements of the reaction of V⁺ + CO₂, ¹⁰ background VO⁺ ions are observed in the present reaction, which are believed to be partly produced by laser ablation of the oxide layer on the surface of the V rod, as well as from chemi-ionization³⁷ reactions between ambient O₂ molecules in the reaction chamber and excited neutral V atoms formed in low-n Ryberg states generated by laser ablation. In this work, the background VO⁺ ion intensities have been carefully corrected for in σ (VO⁺) determinations. The H₂O samples are purchased from Sigma-Aldrich with the quoted purity of \geq 99.96%.

III. RESULTS AND DISCUSSIONS

Illa. Mass Spectra and Reaction Product Channels. Panels a and b of Figure 1 show the mass spectra of the $V^{+}(a^{3}F_{2})$ reactant ion source and the $V^{+}(a^{3}F_{2}) + H_{2}O$ reaction, respectively. Both mass spectra were recorded at $E_{cm} = 3.0 \text{ eV}$, covering the mass to charge ratio (m/z) range 48-70. The mass spectrum of Figure 1a was obtained without filling H₂O reactant gas in the rf-octopole reaction cell, whereas the mass spectrum of Figure 1b was recorded after filling the reaction cell with H₂O vapor at a pressure of 2.0×10^{-4} Torr. In order to show the weak ion peaks more clearly, the mass spectra, except in the region of the very strong ⁵¹V⁺ reactant ion peak, are magnified by 20 times and then shifted up by 20 (shown as the red spectra). In Figure 1a, three peaks are oberved at m/z =50, 51, and 67, which are assigned as ⁵⁰V⁺, ⁵¹V⁺, and VO⁺ ions, respectively. 50V+ is the isotope of 51V+, and the relative intensities for these two isotopes observed are consistent with the known natural isotopic abundances for the V atom.³⁸ Similar to the previous study of the V⁺ + CO₂ reaction, ¹⁰ VO⁺ ions of Figure 1a are observed without H2O filled in the reaction gas cell, indicating that background VO+ ions are formed and that the measured VO+ product ion intensity requires background subtraction. Comparing the mass spectra of Figure 1a,b reveals two product ion peaks at m/z = 52 and 68, which are assigned as product VH+ and VOH+ ions, respectively. In the mass spectrum of Figures 1b, the intensity of the VO⁺ peak at m/z = 68 is found to increase significantly compared with that of Figure 1a. This observation indicates that product VO+ ions are produced from the V+ + H2O reaction. Similar mass spectra are also observed when the reactant V⁺ ions are prepared in the $a^5D_I(J=0,2)$ and $a^5F_I(J=0,2)$ 1, 2) spin-orbit electronic states. The analysis of the mass spectra indicates that three product channels (or product states), VO⁺ + H₂, VH⁺ + OH, and VOH⁺ + H, are formed from each of the reactant states, $V^+(a^5D_I) + H_2O$, $V^+(a^5F_I) +$

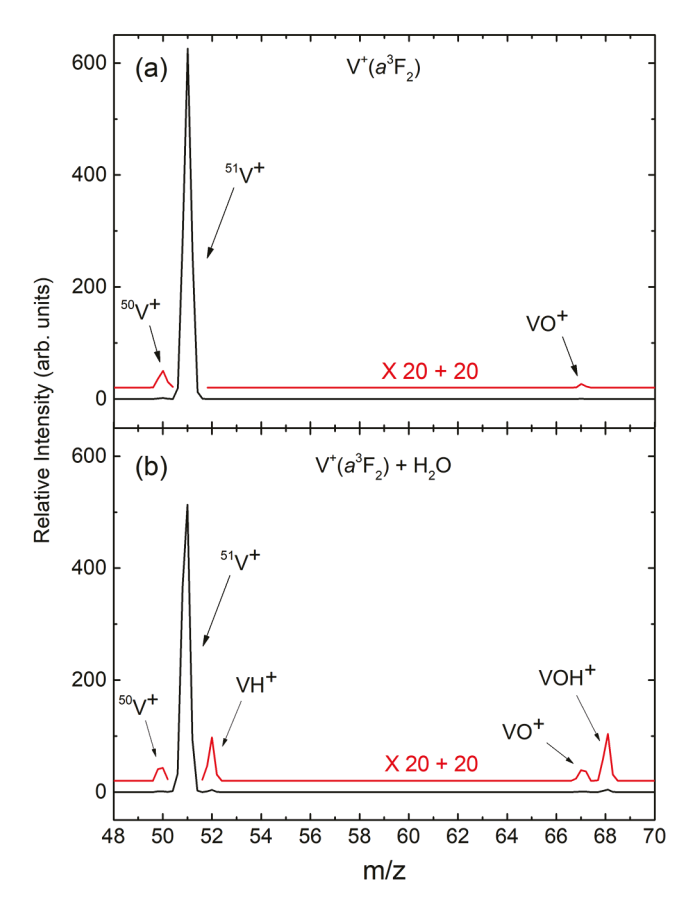


Figure 1. Comparison of mass spectra for the (a) $V^+(a^3F_2)$ reactant ion source and (b) the $V^+(a^3F_2) + H_2O$ reaction. In (a), three peaks are oberved at m/z = 50, 51, and 67, which are labeled as $^{50}V^+, ^{51}V^+$, and VO^+ , respectively. Comparing the mass spectra for (a) and (b) reveals two more product ion peaks at m/z = 52 and 68, which are assigned as VH^+ and VOH^+ , respectively. In addition, the intensity of the VO^+ peak at m/z = 67 in (b) is observed to be significantly enhanced compared to that of (a), indicating VO^+ is a primary product ion of the $V^+(a^3F_2) + H_2O$ reaction. In order to clearly depict the ion peaks with small intensities, the mass spectra except in the region of the $^{51}V^+$ peaks are magnified (by 20 time and then shifted up by 20) and shown in red.

 H_2O , and $V^+(a^3F_J)$ + H_2O , giving rise to a total of nine reactions, as listed in reactions 1–9. Unless specified, all reactant and product species of these reactions are assumed to be in their ground states.

$$V^{+}(a^{3}F_{J}) + H_{2}O \rightarrow VO^{+} + H_{2}$$
 $E_{T} = -2.0 \pm 0.1 \text{ eV}$ (1)

$$V^{+}(a^{5}F_{f}) + H_{2}O \rightarrow VO^{+} + H_{2}$$
 $E_{T} = -1.2 \pm 0.1 \text{ eV}$ (2)

$$V^{+}(a^{5}D_{I}) + H_{2}O \rightarrow VO^{+} + H_{2}$$

$$E_{\rm T} = -0.9 \pm 0.1 \text{ eV}$$
 (3)

$$V^{+}(a^{3}F_{J}) + H_{2}O \rightarrow VH^{+} + OH$$
 $E_{T} = 1.3 \pm 0.1 \text{ eV}$ (4)

$$V^{+}(a^{5}F_{J}) + H_{2}O \rightarrow VH^{+} + OH$$
 $E_{T} = 2.2 \pm 0.1 \text{ eV}$

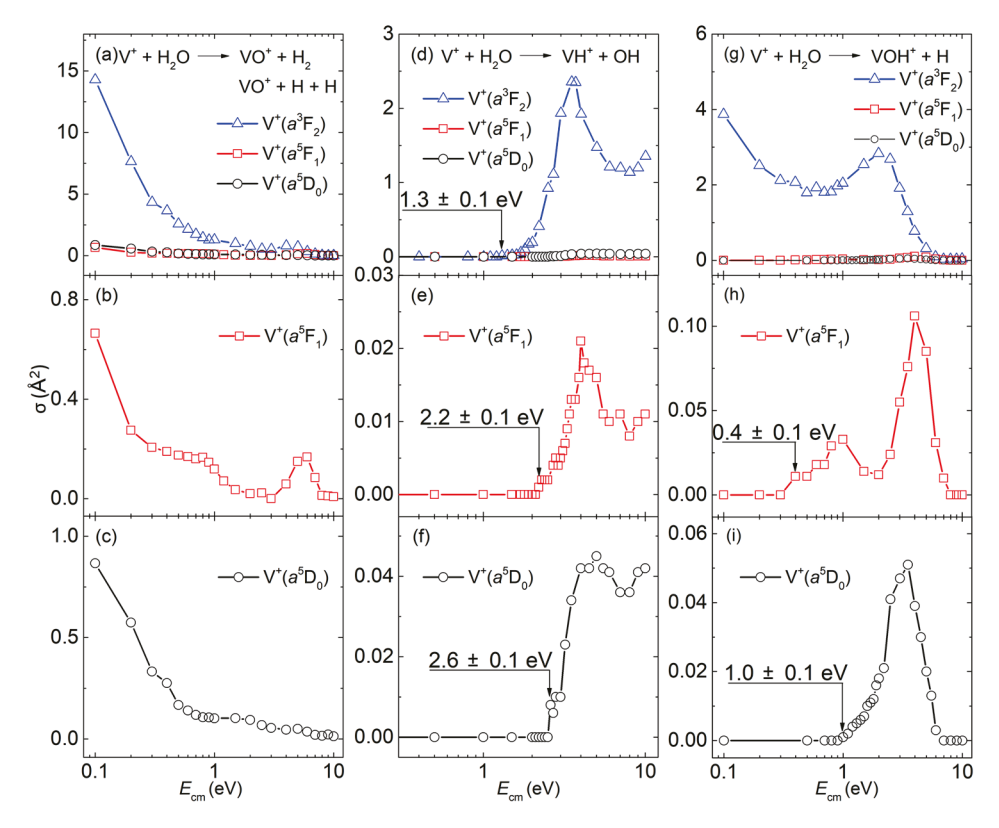


Figure 2. Comparison of $\sigma(VO^+)$ in (a), (b), and (c); $\sigma(VH^+)$ in (d), (e), and (f), and $\sigma(VOH^+)$ in (g), (h), and (i) for the reactions of $V^+(a^3F_{2}, a^5F_1)$, and $a^5D_0 + H_2O$ observed in the E_{cm} range from 0.1 to 10.0 eV. The σ curves of (a), (d), and (g) show the contrast of $\sigma(VO^+)$, $\sigma(VH^+)$, $\sigma(VOH^+)$ when the reactant V^+ ions are preapred in a^3F_2 , a^5F_1 , and a^5D_0 quantum-electronic states, respectively. (b) and (c), (e) and (f), and (h) and (i), are the magnified views of $\sigma(VO^+)$, $\sigma(VH^+)$ and $\sigma(VOH^+)$, when the reactant V^+ ions are preapred in the quintet $V^+(a^5F_1)$ and v^5D_0 0 states, respectively.

(7)

$$V^{+}(a^{5}D_{J}) + H_{2}O \rightarrow VH^{+} + OH$$
 $E_{T} = 2.6 \pm 0.1 \text{ eV}$ (6)
 $V^{+}(a^{3}F_{J}) + H_{2}O \rightarrow VOH^{+} + H$

 $E_{\rm T} = -0.1 \pm 0.2 \text{ eV}$

$$V^{+}(a^{5}F_{f}) + H_{2}O \rightarrow VOH^{+} + H$$
 $E_{T} = 0.4 \pm 0.1 \text{ eV}$ (8)

$$V^{+}(a^{5}D_{J}) + H_{2}O \rightarrow VOH^{+} + H$$
 $E_{T} = 1.0 \pm 0.1 \text{ eV}$ (9)

We have listed in reactions 1-9 their corresponding threshold energies of reaction $(E_T$'s). The reactions with positive (negative) $E_{\rm T}$ values are endothermic (exothermic) reactions. As shown in the previous studies of the V+ D2 (CO_2, CH_4) reactions, 9,10 the endothermicity or positive E_T values can be determined by $E_{\rm cm}$ threshold or $E_{\rm T}$ measurements of the σ curves, as depicted in Figure 2d, e, f, h, i. However, since reactions 1–3 are exothermic, and thus their σ curves do not exhibit distinct E_{cm} thresholds, we have deduced the $E_{\rm T}$ value of -0.9 eV for reaction 3 by using known 0 K heats of formation $(\Delta_i H_0$'s) of the chemical species involved, along with the known D_0 value for VO^+ . $^{10,39-43}$ As pointed out previously, the a⁵F₁ and a³F₂ excited electronic states are known to be higher than the a⁵D₀ ground electronic state by 0.3 and 1.1 eV, respectively. After taking into account these electronic energies, we obtained the $E_{\rm T}$ values as -1.2 eV for reaction 2 and -2.0 eV for reaction 1.

With the exception of the $E_{\rm T}$ value of -0.1 eV assigned for reaction 7, which is deduced from the measured E_T value of 1.0 eV for reaction 9, together with the known electronic energy of -1.1 eV for the excited a^3F_2 state, all other E_T values for reactions 4-6, 8, and 9 are obtained in this work from direct $E_{\rm cm}$ threshold or $E_{\rm T}$ measurements, achieving an error limit of ±0.1 eV. After taking into account this experimental uncertainty, we find that the $E_{\rm T}$ values observed as shown in Figure 2d-i are consistent with the known electronic energy spacings for the a⁵D₀, a⁵F₁, and a³F₂ spin-orbit electronic states. This analysis shows that the formation of VO⁺ + H₂ from reactions 1-3 [Figure 2a-c] and VOH+ + H from reactions 7 [Figure 2g] are exothermic in nature. As expected, their $\sigma(VO^+)$ and $\sigma(VOH^+)$ curves are found to appear as a monotonically decreasing profile as E_{cm} is increased, instead of appearing as a collision-induced-dissociation (CID) peak-like feature with a discernible $E_{\rm cm}$ threshold.

IIIb. Quantum-Electronic-State Effects. Here, we have designated $\sigma(a^3F_2: VO^+)$, $\sigma(a^5F_1: VO^+)$, $\sigma(a^5F_0: VO^+)$, $\sigma(a^3F_2: VH^+)$, $\sigma(a^5F_1: VH^+)$, $\sigma(a^5D_0: VH^+)$, $\sigma(a^3F_2: VOH^+)$, $\sigma(a^5F_1: VOH^+)$, and $\sigma(a^5D_0: VOH^+)$ as the integral cross section curves for reactions 1–9. These σ curves measured in the E_{cm} range 0.1–10 eV are depicted in Figure 2a–i, respectively.

More specifically, Figure 2a shows the direct comparison of the $\sigma(a^5D_0: VO^+)$, $\sigma(a^5F_1: VO^+)$, and $\sigma(a^3F_2: VO^+)$ curves in the same cross section scale, and Figure 2b,c show the magnified views of the $\sigma(a^5F_1: VO^+)$ and $\sigma(a^5D_0: VO^+)$ curves, respectively. Similarly, Figure 2d [Figure 2g] displays the direct comparison of $\sigma(a^5D_0: VH^+)$, $\sigma(a^5F_1: VH^+)$, and $\sigma(a^3F_2: VH^+)$

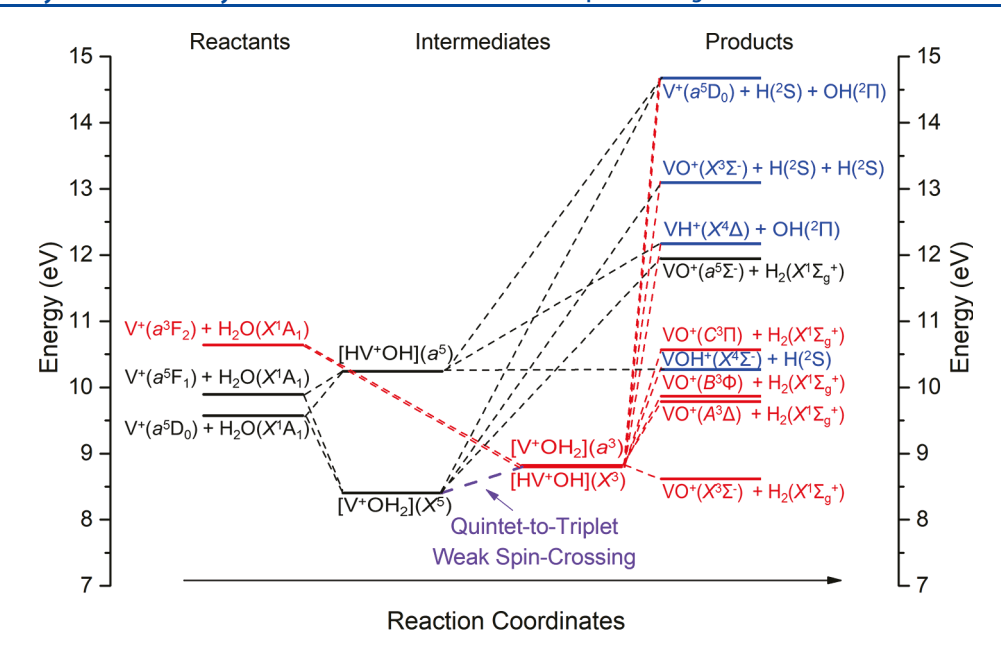


Figure 3. Schematic energy level diagram for the of $V^+ + H_2O$ reaction system in the heat-of-formation scale. The left side column shows the reactant states, $V^+(a^3F_2) + H_2O(X^1A_1)$, $V^+(a^5F_1) + H_2O(X^1A_1)$, and $V^+(a^5D_0) + H_2O(X^1A_1)$; the middle columns are the energy levels of the reaction intermediates predicted by recent theoretical DFT calculations. The quintet intermediates $[V^+OH_2](X^5)$ and $[HV^+OH](a^5)$ are in black while the triplet ones $[HV^+OH](X^3)$ and $[V^+OH_2](a^3)$ are in red. Possible products channels are depicted on the right side with red, black, or blue lines on the basis of their multiplicities. The weak quintet-to-triplet spin-crossing is shown schematically along the reaction coordinates by the purple dashed line connecting the quintent and triplet reaction intermediates.

[σ(a⁵D₀: VOH⁺), σ(a⁵F₁: VOH⁺), and σ(a³F₂: VOH⁺)]; and Figure 2e,f [Figure 2h,i] show the magnified views of σ(a⁵F₁: VH⁺) and σ(a⁵D₀: VH⁺) [σ(a⁵F₁: VOH⁺) and σ(a⁵D₀: VOH⁺)], respectively. The comparisons of the σ curves of Figure 2a,d,g clearly show that in the $E_{\rm cm}$ range of 0.1–10.0 eV, the σ values for the triplet product channels are overwhelmingly greater than those for the quintet product channels. The fact that these σ curves cover the absolute integral cross section range of more than 4 orders of magnitude indicates that the detection sensitivity achieved in the present state-selected σ measurements is extremely high.

As pointed out above, for all $\sigma(VO^+)$, $\sigma(VH^+)$, and $\sigma(VOH^+)$ curves shown in Figure 2a,d,g, respectively, the triplet V⁺(a³F₂) ion exhibits overwhelmingly higher chemical reactivity toward H₂O than that for the two quintet V⁺(a⁵D₀ and a^5F_1) ions. Since the σ values for the quintet $V^+(a^5D_0)$ and $V^{+}(a^{5}F_{1})$ ions + $H_{2}O$ reaction are similar, only the $\sigma(a^{5}D_{0})$ are chosen for a more detailed comparison with the $\sigma(a^3F_2)$ as given below. We find that for the VO+ + H2 product channel, $\sigma(a^3F_2: VO^+)$ is about 18, 15, 13, 15, and 1 times $\sigma(a^5D_0:$ VO^{+}) at $E_{cm} = 0.1$, 0.5, 1.0, 5.0, and 10.0 eV, respectively. For the VH⁺ + OH product channel, $\sigma(a^3F_2: VH^+)$ is about 115, 33, and 32 times $\sigma(a^5D_0: VH^+)$ at $E_{cm} = 2.5$, 5.0, and 10.0 eV, respectively. For the VOH⁺ + H product channel, $\sigma(a^3F_2)$: VOH⁺) is about 65, 15, and 1 times $\sigma(a^5D_0: VOH^+)$ at $E_{cm} =$ 2.5, 5.0, and 10.0 eV, respectively. These comparisons clearly show that the triplet a^3F_2 state is dominantly more reactive than the two quintet a⁵D₀ and a⁵F₁ states in activating the H₂O

As pointed out above, two reaction intermediates have been proposed that may play a role in the $V^+ + H_2O$ reaction. One intermediate was suggested to have the $C_{2\nu}$ V^+OH_2 ion—molecule complex structure formed by charge—dipole and induced dipole attractions between the V^+ ion and the H_2O molecule. The other intermediate was proposed to have the

inserted HV⁺OH structure formed by V⁺ insertion into an O–H bond of the $\rm H_2O$ molecule. In the long range, the main interaction between the reactant V⁺ ion and the $\rm H_2O$ molecule is expected to be the charge—dipole attraction, with the net negative charge residing at the O atom of the $\rm H_2O$ molecule. Thus, when reactant V⁺ ion approaches the $\rm H_2O$ molecule, it may prefer to attack the O atom end instead of the two terminal H atoms of the $\rm H_2O$ molecule. This interaction may induce the formation of the VO⁺ bond, which is known to be a strong bond with a bond energy of about 6 eV. 10,42,43 Concomitantly, the VO⁺ bond formation could weaken the OH bonds of the V⁺OH₂ intermediate, inducing the two terminal H atoms to combine, giving rise to the VO⁺ + $\rm H_2$ product channel via $\rm H_2$ elimination.

The insertion intermediate HV+OH can be generated by cleavaging one OH bond of the H2O molecule and forming two new bonds, V+-H or V+-OH, and thus, it is also energetically favorable.²⁷ The formation of the ion-molecule complex as well as the inserted intermediates can both give rise to the formation of VH⁺ and VOH⁺ product ions via a reaction complex mechanism at low E_{cm} values. The earlier spectroscopic study of Lessen et al. suggested the involvement of the $C_{2\nu}$ V⁺OH₂ ion-molecule intermediate, ⁴⁴ and this result is supported by the later IR spectroscopic study based on the Artagging techniques. 44,45 In this same IR spectroscopic study, the authors declared no evidence was found for the involvement of the inserted intermediate HV+OH. Nevertheless, earlier mass spectrometric and theoretical investigations on the V+ + H2O reaction had long proposed the insertion intermediate HV+OH as the major reaction intermediate.^{27,28} Our observations in the present work are consistent with the involvement of both reaction intermediates, which will be dicussed in more detail in the following section.

IIIc. Schematic Energy Level Diagram for the $V^+(a^5D_0, a^5F_1, and a^3F_2) + H_2O$ Reactions. Figure 3 depicts a

schematic energy level diagram for the $V^+(a^5D_0, a^5F_1, and a^3F_2)$ + $H_2O(X^1A_1)$ reactions in the heat of formation scale. The presentation of this diagram is aimed to bring out the correlations between the reactant states and product states according to the conservation of total electron spins. A similar energy level diagram was presented previously in the report of the V⁺(a^5D_0 , a^5F_1 , and a^3F_2) + CO₂(CH₄) reactions.¹⁰ On the left side of Figure 3, the three reactant states, V+(a5D₁) + $H_2O(X^1A_1)$, $V^+(a^5F_I) + H_2O(X^1A_1)$, and $V^+(a^3F_I) + H_2O$ (X¹A₁), are marked in black (quintet), black (quintet), and red (triplet), respectively. On the right side of Figure 3, the possible product states are highlighted with the same color rule: i.e., black for quintet states and red for triplet states. Since the dominant product channel for the V+ + H2O reaction system is $VO^+ + H_2$, and the energetics for the $VO^+(X^3\Sigma^-)$, $A^3\Delta$, $B^3\Phi$, and $C^3\Pi$) electronic states are known, ^{41,42} we have included the excited product states, $VO^{+}(A^{3}\Delta) + H_{2}(X^{1}\Sigma_{g}^{+})$, $VO^+(B^3\Phi) + H_2(X^1\Sigma^+)$, and $VO^+(C^3\Pi) + H_2(X^1\Sigma_{\sigma}^+)$, in the energy level diagram, in addition to the $VO^+(X^3\Sigma^-)$ + $H_2(X^1\Sigma_g^+)$ ground product state. All these product states are highlighted in red because they are all triplet states. The other two product states, $VH^+(X^4\Delta) + OH(^2\Pi)$ and $VOH^+(X^4\Sigma^-) +$ H(2S), which can correlate with both triple and quintet reactant states, are marked in blue. In addition, we have also depicted in Figure 3 the dissociative product states, $VO^{+}(X^{3}\Sigma^{-}) + H(^{2}S) + H(^{2}S)$ and $V^{+}(a^{5}D_{0}) + H(^{2}S) +$ $OH(^{2}\Pi)$. Marking the product states in blue color is also to show that these product states can be produced by "weak quintet-triplet crossing" interactions. We note that the first excited quintet $VO^+(a^5\Sigma^-) + H_2$ product state, which can correlate directly with the $V^+(a^5D_0)^+ + H_2O$ and $V^+(a^5F_1)^+ + H_2O$ reactant states, $^{39-41}$ is at an energy of about 2.1 eV higher than the latter quintet reactant states.

In the middle columns of Figure 3, we also show the previous DFT calculated energy positions for the proposed reaction intermediates. According to this calculation,²⁸ the V⁺OH₂ intermediate has a quintet V⁺OH₂(X⁵) ground state, which is about 0.9 eV lower than its excited triplet $V^+OH_2(a^3)$ state, whereas the inserted HV+OH intermediate has a triplet $HV^+OH(X^3)$ ground state, which is about 1.4 eV lower than its excited quintet HV+OH(a⁵) state. Furthermore, the quintet $V^+OH_2(X^5)$ intermediate is about 2.3 eV lower than that of the quintet HV+OH(X5) intermediate. Therefore, when the reactant V+ ion is initially prepared in a quintet reactant electronic state, $V^+(a^5D_0) + H_2O$ or $V^+(a^5F_1) + H_2O$, the connection to the quintet V⁺OH₂(X⁵) intermediate would be preferred rather than to the quintet HV⁺OH(X⁵) intermediate. As discussed above, the former intermediate mainly leads to the formation of VO+ while the later gives rise to VH+ and VOH⁺. Thus, $\sigma(VH^+)$ and $\sigma(VOH^+)$ from quintet $V^+(a^5D_0)$ + H_2O and $V^+(a^5F_1) + H_2O$ reactant states are suppressed due to the unfavorable connection to the quintet HV+OH(X5) intermediate. In addition, the formation of the preferred quintet V+OH2(X5) intermediate is not expected to lead to high $\sigma(VO^+)$ from the two quintet $V^+(a^5D_0) + H_2O$ and $V^{+}(a^{5}F_{1}) + H_{2}O$ reactant states, because the first correlated excited quintet $VO^+(a^5\Sigma^-) + H_2$ product state, which can directly linked by spin conservation, is at 2.4 and 2.1 eV above the $V^+(a^5D_0) + H_2O$ and $V^+(a^5F_1) + H_2O$ reactant states, $^{39-41}$ respectively. A "quintet-to-triplet spin crossing" is needed for the reactant state with quintet multiplicity to form VO+ with triplet multiplicity. The low value observed of $\sigma(a^5D_0)$ or a^5F_1 : VO+) indicates that the "quintet-to-triplet spin crossing" is

weak. Therefore, all three reaction product channels $\sigma(VO^+)$, $\sigma(VH^+)$, and $\sigma(VOH^+)$ for the reaction of $V^+ + H_2O$ are inhibited when reactant V^+ ions are prepared in the quintet states of a^5D_0 and a^5F_1 , due to the reaction mechanism of favoring the conservation of the total electron spins.

When the reactant V^+ ion is prepared in the triplet a^3F_2 electronic state, it gives the triplet $V^+(a^3F_2) + H_2O$ reactant state, and the correlation diagram shows that it can lead to the formation of the triplet V⁺OH₂(a³) and HV⁺OH(X³) intermediates with little preference as these two triplet intermeidates are predicted to have similar energies. Without any crossing of reaction surfaces of different multiplicities. these two triplet intermediates can further evolve to the product states of VO⁺ + H₂, VH⁺ + OH, and VOH⁺ + H with the total electron spin conserved to be one. The present experiment shows that when such processes are energetically allowed, $\sigma(VO^+)$, $\sigma(VH^+)$, and $\sigma(VOH^+)$ for the $V^+(a^3F_2)$ + H₂O reactions are observed to be much enhanced compared to that for the $V^+(a^5D_0$ and $a^5F_1) + H_2O$ reactions, indicating that the reaction mechanism of total electron spin conservation is highly favored for the titled reaction.

IIId. Bond Dissociation Energies, $D_0(V^+-H)$ and $D_0(V^+-OH)$. As illustrated in previous studies, 9,10 the positive E_T value of a chemical reaction channel determined by the E_{cm} threshold measurement of the state-selected σ curve can be used to deduce the $D_0(V^+-H)$ and $D_0(V^+-OH)$ values. On the basis of thermochemical cycles, we can obtain the relationships as listed in eqs 10-12. We can show that the D_0 values are related to E_T at T=0 (or E_0) through these equations.

$$D_0(V^+-H) = \Delta_f H_0(V^+) + \Delta_f H_0(H) - \Delta_f H_0(VH^+)$$
(10)

$$D_0({\rm H-OH}) = \Delta_{\rm f} H_0({\rm H}) + \Delta_{\rm f} H_0({\rm OH}) - \Delta_{\rm f} H_0({\rm H_2O})$$
(11)

$$E_0 = [\Delta_f H_0(VH^+) + \Delta_f H_0(OH)] - [\Delta_f H_0(V^{+*}) + \Delta_f H_0(H_2O)]$$
(12)

Here, $\Delta_i H_0(V^+)$ in eq 10 is the 0 K heat of formation of V^+ in the ground state and $\Delta_i H_0(V^{+*})$ in eq 12 is that in the selected electronic state of a^3F_2 , a^5F_1 , or a^5D_0 . By combining the above eqs 10–12, we can obtain eq 13,

$$D_0(V^+-H) = D_0(H-OH) - E_0$$
$$- [\Delta_f H_0(V^{+*}) - \Delta_f H_0(V^+)]$$
(13)

Since $D_0(H-OH)$ is well-known as 5.101 \pm 0.001 eV and $[\Delta_t H_0(V^{+*}) - \Delta_t H_0(V^{+})]$ is the electronic excitation energy of the reactant V^{+*} ion, which are known to be 1.1, 0.3, and 0.0 eV for a^3F_2 , a^5F_1 , and a^5D_0 , respectively, the $D_0(V^+-H)$ can be deduced readily using the E_0 value. However, the $E_{\rm cm}$ threshold measurement of the present study gives the $E_{\rm T}$ value. In order to use the E_0 value, it is necessary to convert E_T to E_0 . As listed in reactions 4–6, the E_T 's for the formation of the VH⁺ + OH product channel from the $V^+(a^3F_2) + H_2O$, $V^+(a^5F_1) + H_2O$, and $V^+(a^5D_0) + H_2O$ reaction are 1.3 \pm 0.1, 2.2 \pm 0.1, and 2.6 \pm 0.1 eV, respectively. Thus, assuming that $E_0 \approx E_T$, the $D_0(V^+-H)$ can be deduced correspondingly as 2.7 ± 0.1 , 2.6 ± 0.1 0.1, and 2.5 \pm 0.1 eV. Taking the average of these three measurements, we have $D_0(V^+-H) = 2.6 \pm 0.2$ eV. This value is in excellent agreement with the value of $D_0(V^+-D) = 2.56 \pm$ 0.20 eV reported recently. Similar to the $D_0(V^+-D)$ measurement in the recent $V^+ + D_2$ study, we have assigned an error limit of ± 0.20 eV on the basis of general comparisons between well-known energetic values available in the literatures and measurements obtained using the present experimental scheme.

A similar relation can be derived for $D_0(V^+-OH)$, as given by eq 14.

$$D_0(V^+-OH) = D_0(H-OH) - E_0$$
$$- [\Delta_f H_0(V^{+*}) - \Delta_f H_0(V^+)]$$
(14)

As shown in Figure 2h,i, the $E_{\rm T}$'s for product channel VOH⁺ + H from reactions 8 and 9 are determined as 0.4 ± 0.1 and 1.0 ± 0.1 eV, respectively. Thus, by using eq 14 and assuming that $E_0 \approx E_{\rm T}$, the $D_0({\rm V}^+{\rm -OH})$ can be deduced to be 4.4 ± 0.1 and 4.1 ± 0.1 eV, respectively. On the basis of these results, we obtain the averaged upper bound value of $D_0({\rm V}^+{\rm -OH}) = 4.3 \pm 0.2$ eV.

We emphasize that the direct D_0 determination as shown in eqs 10-14 requires the E_0 instead of the $E_{\rm T}$ measurement. The most important thermal energy correction for the conversion of $E_{\rm T}$ to E_0 measurement is expected to be the thermal energy of the reactant $H_2{\rm O}$ molecule, in this case. Since the thermal energy for $H_2{\rm O}$ has not been properly accounted and corrected for in the above thermochemical analyses and derivation, all the D_0 values deduced above associated with the reaction systems of ${\rm V^+} + {\rm D_2(CO_2, CH_4)}$ are upper bound values, which are found to be higher than the accepted corresponding literature values by $\approx 0.3-0.5$ eV. That is, following the procedures for data analysis as given above, we obtained $D_0({\rm V^+}-{\rm H}) \leq 2.6 \pm 0.2$ eV and $D_0({\rm V^+}-{\rm OH}) \leq 4.3 \pm 0.2$ eV, which are upper bound values.

Ille. Kinetic Energy Effects. Kinetic energy (E_{cm}) effects on $\sigma(\text{VO}^+)$, $\sigma(\text{VH}^+)$, and $\sigma(\text{VOH}^+)$ for the $V^+(\text{a}^5\text{D}_0)$; a^5F_1 ; $\text{a}^3\text{F}_2) + \text{H}_2\text{O}$ reactions can also be observed in panels a-c, d-f, and g-i of Figure 2, respectively. The distinct $\sigma(\text{a}^3\text{F}_2\text{: VO}^+)$, $\sigma(\text{a}^5\text{F}_1\text{: VO}^+)$, $\sigma(\text{a}^5\text{F}_1\text{: VO}^+)$, $\sigma(\text{a}^5\text{F}_1\text{: VH}^+)$, $\sigma(\text{a}^5\text{F}_1\text{: VOH}^+)$, and $\sigma(\text{a}^5\text{D}_0\text{: VOH}^+)$ curves obtained in the E_{cm} range 0.1–10.0 eV reveal that, similarly to internal electronic-state energy, E_{cm} can also couple effectively with the internal reaction coordinates of the $V^+(\text{a}^5\text{D}_0; \text{a}^5\text{F}_1; \text{a}^3\text{F}_2) + \text{H}_2\text{O}$ reactions in promoting chemical reactivity.

All three $\sigma(VO^+)$ curves depicted in Figure 2a-c, are known to associate with exothermic reaction product channels with negative E_T values, as listed in reactions 1-3. As expected, the $\sigma(a^5D_0, a^5F_1, \text{ and } a^3F_2: VO^+)$ curves are all found to decrease nearly exponentially as $E_{\rm cm}$, is increased. This finding is in general accord with the prediction of the Langevin-Gioumousis-Stevenson (LGS) orbiting model. 46,47 The exothermic nature of the $\sigma(a^5D_0, a^5F_1, and a^3F_2: VO^+)$ curves observed here confirms the formation of the VO⁺($X^3\Sigma^-$) + H₂ product state. The observation of the LGS cross section profiles also suggests that the reactions involved are governed by attractive potential energy surfaces and proceed via a reaction complex mechanism at low E_{cm} values. While the $\sigma(a^3F_2: VO^+)$ and $V^+(a^5D_0: VO^+)$ curves exhibit relatively smooth LGS cross section profiles, the $\sigma(a^5F_1: VO^+)$ curve resolves two notable bumps at $E_{\rm cm} = 0.3-1.5$ and 3.0-7.0 eV superimposing on the LGS cross section curve. The nature for the weaker bump at $E_{\rm cm} = 0.3-1.5$ eV is not known. We have tentatively assigned the stronger bump at $E_{cm} = 3.0-7.0$ eV to the formation of the reaction product channel VO $^+$ (X $^3\Sigma^-$) +

 $H(^2S) + H(^2S)$ from the $V^+(a^5F_1) + H_2O$ reactant state on the basis of known E_0 values of 3.5, 3.2, and 2.4 eV, for reaction 15 with reactant V^+ prepared in respective a^5D_0 , a^5F_1 , and a^5F_2 states.

$$V^{+}(a^{5}D_{0}; a^{5}F_{1}; a^{3}F_{2}) + H_{2}O(X^{1}A_{1}) \rightarrow VO^{+}(X^{3}\Sigma^{-})$$

+ $H(^{2}S) + H(^{2}S)$ $E_{0} = 3.5, 3.2, 2.4 \text{ eV}$ (15)

We note that the product states resulting from collision-induced dissociation (CID) reactions, as shown in reaction 16, become energetically accessible at $E_{\rm cm} > 5.1$ eV for the reactant V⁺ ion prepared in the V⁺(a⁵D₀) ground state.

$$V^{+}(a^{5}D_{0}) + H_{2}O(X^{1}A_{1}) \rightarrow V^{+}(a^{5}D_{0}) + OH(^{2}\Pi)$$

+ $H(^{2}S)$ $E_{0} = 5.1 \pm 0.1 \text{ eV}$ (16)

The possible reaction product states of reactions 15 and 16 are included in the top right side of the energy level diagram of Figure 3. These dissociative reactions are likely responsible for the observed decay of the $\sigma(VH^+)$, and $\sigma(VOH^+)$ curves at $E_{cm} > 5.1$ eV.

Even though the absolute values of $\sigma(a^3F_2: VH^+)$ are predominantly higher than those of $\sigma(a^5D_0: VH^+)$ and $\sigma(a^5F_1: VH^+)$ by factors of 50-100 at the same E_{cm} values, it is interesting to find that the overall profiles of these σ curves appear to be very similar. At E_{cm} above the E_T threshold, $\sigma(VH^+)$ is found to increase rapidly as E_{cm} is increased, and the σ value reaches the peak value at E_{cm} about 2 eV higher than the E_{cm} threshold. Then $\sigma(VH^+)$ begins to decline as E_{cm} is increased until $E_{cm}=8.0$ eV. At $E_{cm}=8.0$ eV, the further increase of $\sigma(VH^+)$ is evident as E_{cm} is further increased. Comparing the $\sigma(VH^+)$, $\sigma(VO^+)$, and $\sigma(VOH^+)$ curves at $E_{cm}>8.0$ eV in Figure 2a-i, $\sigma(VH^+)$ is the only product channel remaining with nonzero cross sections. The nonvanishing $\sigma(VH^+)$ values observed at $E_{cm}>8.0$ eV can be attributed to the formation of product VH^+ ions in excited electronic states.

Different from the $\sigma(VO^+)$ and $\sigma(VH^+)$ curves presented above, which consist of either totally exothermic or endothermic product channels, respectively, the $\sigma(VOH^+)$ curves for the VOH+ + H reaction product channel display a mix of exothermic and endothermic characters. A careful comparison of the $\sigma(a^3F_2: VOH^+)$, $\sigma(a^5F_1: VOH^+)$, and $\sigma(a^5D_0: VOH^+)$ curves depicted in Figure 2g-i, respectively, reveals interesting evolution trends of the σ curves as the V⁺ electronic state is changed. The $\sigma(a^5D_0: VOH^+)$ and $\sigma(a^5F_1:$ VOH⁺) curves show the endothermic behavior with distinct $E_{\rm T}$ values observed at 1.0 \pm 0.1 and 0.4 \pm 0.1 eV, respectively. The $\sigma(a^3F_2: VOH^+)$ curve does not exhibit a E_{cm} threhold, instead it manifests as a LGS cross section curve, which is consistent with the exothermic nature of this product channel. We note that these $E_{\rm cm}$ thresholds obtained for $\sigma(a^5D_0: VOH^+)$ and $\sigma(a^5F_1: VOH^+)$ differ by about 0.6 eV, which is larger than the known energy difference of 0.3 eV between the a⁵D₀ and a⁵F₁ states of V⁺. This observation may indicate that the E_{cm} threshold of 1.0 \pm 0.1 eV for $\sigma(a^5D_0: VOH^+)$ is too high, possibly due to the existence of a potential barrier for the $\sigma(a^5D_0: VOH^+)$. It should be noted that this indication may lead to a smaller value (by $\sim 0.1-0.3$ eV) of $D_0(V^+-OH)$.

The $\sigma(a^3F_2: VOH^+)$ curve of Figure 2g can be decomposed into contributions from exothermic and an endothermic components. The exothermic component is manifested as a LGS-type cross section curve and the endothermic component appears as a large bump in the $E_{\rm cm}$ range 0.8–7.0 eV with the

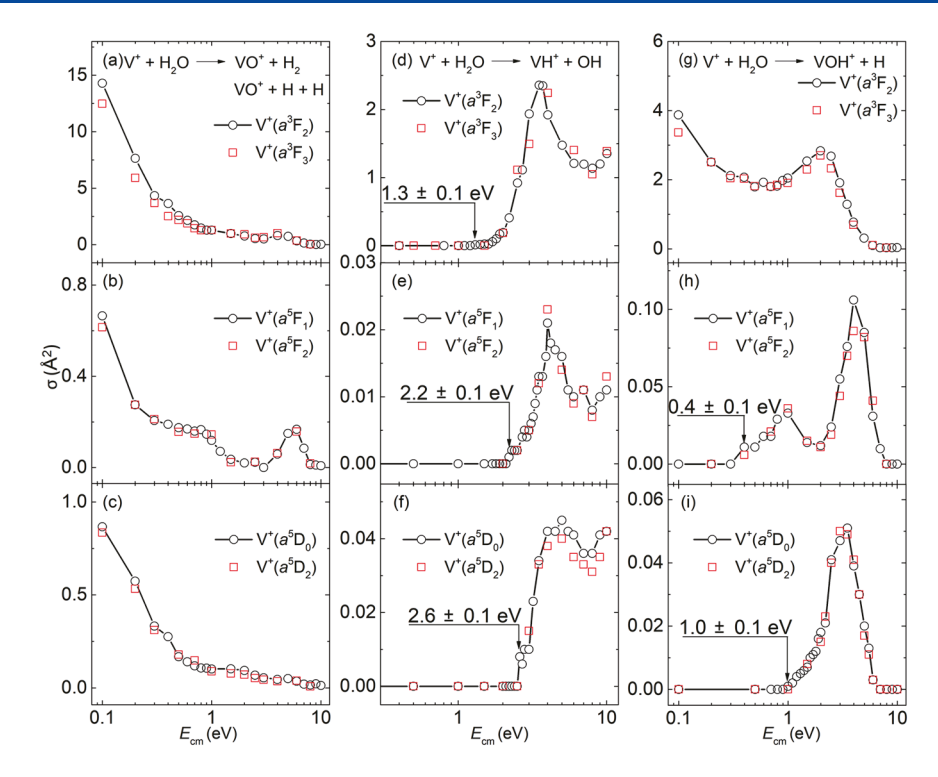


Figure 4. Investigation of the *J*-state dependences for the reaction system of V⁺($a^3F_{2,3}$, $a^5F_{1,2}$, and $a^5D_{0,2}$) + H₂O. Comparisons of (a) $\sigma(a^3F_2: VO^+)$ versus $\sigma(a^3F_3: VO^+)$, (b) $\sigma(a^5F_1: VO^+)$ versuss $\sigma(a^5F_2: VO^+)$, (c) $\sigma(a^5D_0: VO^+)$ versus $\sigma(a^5D_2: VO^+)$, (d) $\sigma(a^3F_2: VH^+)$ versus $\sigma(a^3F_3: VH^+)$, (e) $\sigma(a^5F_1: VH^+)$ versus $\sigma(a^5F_2: VH^+)$, (f) $\sigma(a^5D_0: VH^+)$ versus $\sigma(a^5F_2: VOH^+)$, (g) $\sigma(a^3F_2: VOH^+)$ versus $\sigma(a^3F_3: VOH^+)$, (h) $\sigma(a^5F_1: VOH^+)$ versus $\sigma(a^5F_2: VOH^+)$, and (i) $\sigma(a^5D_0: VOH^+)$ versus $\sigma(a^5D_0: VOH^+)$. The results show no *J*-state dependence for the titled reaction system.

peak position appearing near $E_{\rm cm}=2.0$ eV. Although the $E_{\rm cm}$ threshold of this bump cannot be accurately determined due to its overlap with the exothermic component, the profile of this bump observed is consistent with the endothermic nature. As pointed out above, the electronic energies of the a^5F_1 and a^3F_2 states are 0.3 and 1.1 eV higher, respectively, than that of the a^5D_0 ground state. The observation of the exothermic behavior for $\sigma(a^3F_2\colon VOH^+)$ and endothermic behavior for $\sigma(a^5F_1\colon VOH^+)$ indicates that the crossover between endothermic and exothermic behaviors is in the electronic energy range 0.3–1.1 eV for $\sigma(a^5D_0\colon VOH^+)$.

For $\sigma(a^5D_0: VOH^+)$ [Figure 2i], only one peak at $E_{cm} = 1.0-$ 6.0 eV is observed with the peak position situated at $E_{\rm cm} \approx 3.5$ eV, while $\sigma(a^5F_1: VOH^+)$ [Figure 2h] reveals two σ peaks: the weaker one is located at $E_{\rm cm}$ = 0.4–1.5 eV with the σ peak position at $E_{\rm cm} \approx 1.0$ eV and the stronger one is at $E_{\rm cm} = 2.0$ 7.0 eV with the peak position around 4.0 eV. We have also observed a strong peak at $E_{\rm cm}$ = 0.8–7.0 eV for $\sigma({\rm a^3F_2:VOH^+})$ [Figure 2g], which may involve the formation of excited VOH+ ion. The comparison of the $\sigma(a^3F_2: VOH^+)$, $\sigma(a^5F_1: VOH^+)$, and $\sigma(a^5D_0: VOH^+)$ curves of Figure 2g-i, respectively, shows that these σ curves exhibit distinct features and reveals strong dependences on the quantum-electronic state of the reactant V⁺ ion. This observation supports the conclusion that the electronic-state selections for V⁺ have achieved high purity and that the lifetimes of these excited electronic states are longer than the experimental measurement cycles as predicted by the parity and electron spin selection rules. 6,7,10

As pointed out above, the $\sigma(a^3F_2: VOH^+)$, $\sigma(a^5F_1: VOH^+)$, and $\sigma(a^5D_0: VOH^+)$ curves represent the respective chemical reactivity when the reaction occurs in the V⁺(a^3F_2 , a^5F_1 , and a^5D_0) states with electronic energies of 1.1, 0.3, and 0.0 eV. This experiment also illustrates that changing the electronic

state of the V⁺ ion as well as the $E_{\rm cm}$ can alter effectively the ion—molecule reaction dynamics, and thus the chemical reactivity of the V⁺(a⁵D_J, a⁵F_J, and a³F_J) + H₂O reactions. Here, we show that increasing the eletronic energy from 0.0 to 1.1 eV can effectively change the ion—molecule reaction dynamics from a CID-type to a LGS-type. Interestingly, the σ (a⁵F₁: VOH⁺) curve obtained with an electronic energy of 0.3 eV, which is between those of the V⁺(a³F₂ and a⁵D₀) states, is found to exhibit a partially cutoff σ (a⁵F₁: VOH⁺) curve component in Figure 2h compared to that in Figure 2g.

IIIf. Spin–Orbit *J***-State Dependences.** The comparisons of the σ curves for the reactions of V⁺(a⁵D₀ versus a⁵D₂, a⁵F₁ versus a⁵F₂, and a³F₂ versus a³F₃) with H₂O are shown in Figure 4a-i, respectively. Similar to those observed in the studies of the $V^+ + D_2(CO_2, CH_4)$ reactions, 9,10 no discernible *I*-state effects are observed on chemical reactivity of the V⁺ + H₂O reaction. This result indicates that the coupling between electron spin and orbital angular momenta of V+ is also not strong enough for this reaction to show a reactivity effect. Nevertheless, this observation is consistent with the observation that the V⁺ ion manifests strong quantum-electronic-state effects on its chemical reactivity with the H₂O molecule. It is well-known that spin-orbit coupling can facilitate the coupling of different quantum-electronic states of atomic TM cations. 13,48 The fact that different quantum-electronic states of the V⁺ ion are found to exhibit distinct chemical reactivity of V⁺ toward the H₂O molecule indicates that the coupling between different electronic states is weak. Combining all these observations together, we can conclude that, for the $V^+ + H_2O$ reaction, electron spin (or electron multiplicity) rather than the *I* state is the dominant factor for determining the chemical reactivity of the V⁺ ion.

IIIg. $\sigma(a^3F_2$: sum), $\sigma(a^5F_1)$: sum), and $\sigma(a^5D_0$: sum). Figure 5a shows the sum of σ values for all product channels

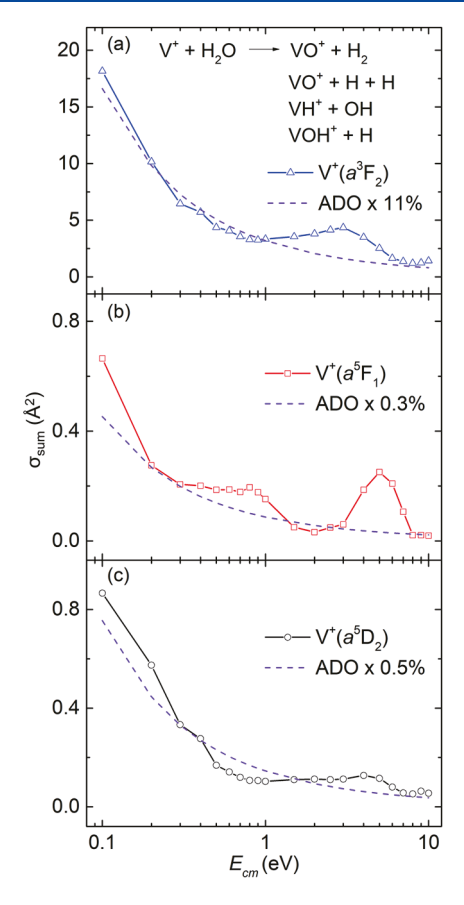


Figure 5. Comparison of (a) $\sigma(a^3F_2: sum)$, (b) $\sigma(a^5F_1: sum)$, and (c) $\sigma(a^5D_0: sum)$ for a reaction system of V⁺(a^3F_2 , a^5F_1 , and a^5D_0) + H₂O in the E_{cm} range from 0.1 to 10.0 eV. Here, $\sigma(a^3F_2: sum) = \sigma(a^3F_2: VO^+) + \sigma(a^3F_2: VH^+) + \sigma(a^3F_2: VOH^+)$; $\sigma(a^5F_1: sum) = \sigma(a^5F_1: VO^+) + \sigma(a^5F_1: VH^+) + \sigma(a^5F_1: VOH^+)$; and $\sigma(a^5D_0: sum) = \sigma(a^5D_0: VO^+) + \sigma(a^5D_0: VH^+) + \sigma(a^5D_0: VOH^+)$. The theorical estimates based on the average-dipole-oritention (ADO) model are shown in a dashed purple line. The scaled factors for $\sigma(ADO)$ are 11%, 0.3%, and 0.5% for $\sigma(a^3F_2: sum)$, $\sigma(a^5F_1: sum)$, and $\sigma(a^5D_0: sum)$, respectively.

from the reaction of V⁺(a³F₂) + H₂O in the E_{cm} range 0.1–10.0 eV. As listed in Figure 5a, the sum of the product channels includes VO⁺ + H₂ as well as possible VO⁺ + H + H, VH⁺ + OH, and VOH⁺ + H. Thus, the $\sigma(a^3F_2: sum)$ curve of Figure 5a is mainly the sum of the $\sigma(a^3F_2: VO^+)$ curve for reaction 1, $\sigma(a^3F_2: VH^+)$ curve for reaction 4, and $\sigma(a^3F_2: VOH^+)$ curve for reaction 7. Similarly, the $\sigma(a^5F_1: sum)$ curve of Figure 5b is mainly the sum of the $\sigma(a^5F_1: VO^+)$ curve for reaction 2, $\sigma(a^5F_1: VH^+)$ curve for reaction 5, and $\sigma(a^5F_1: VOH^+)$ curve for reaction 8. The $\sigma(a^5D_0: sum)$ curve of Figure 5c is mainly the sum of the $\sigma(a^5D_0: VO^+)$ curve for reaction 3, $\sigma(a^5D_0: VH^+)$ curve for reaction 6, and $\sigma(a^5D_0: VOH^+)$ curve for reaction 9.

As shown in Figure 5a–c, the $\sigma(a^3F_2: sum)$, $\sigma(a^5F_1): sum)$, and $\sigma(a^5D_0: sum)$ are found to be nearly the same with nearly identical features compared to the corresponding $\sigma(a^5D_0, a^5F_1, and a^3F_2: VO^+)$ curves shown in Figure 2a–c. This observation is again in accord with the conclusion that $\sigma(a^5D_0, a^5F_1, and a^3F_2: VO^+)$ are the dominant product channels. In flow tube studies, ²⁹ where the reaction rates for individual product

channels were not measured, these $\sigma(a^3F_2:sum)$, $\sigma(a^5F_1:sum)$, and $\sigma(a^5D_0:sum)$ curves can be used to compare with the total rate constant curves obtained as a function of kinetic energy or temperature.

We have attempted to fit the $\sigma(a^3F_2:sum)$, $\sigma(a^5F_1:sum)$, and $\sigma(a^5D_0:sum)$ curves on the basis of the generally scaled theoretical average-dipole-orientation (ADO) model, 47 shown as dashed purple curves in Figure 5a—c. The scaled factors used for the $\sigma(ADO)$ fits are 11%, 0.3%, and 0.5% for the $\sigma(a^3F_2:sum)$, $\sigma(a^5F_1:sum)$, and $\sigma(a^5D_0:sum)$, respectively. On the basis of this comparison, we may conclude that the ADO model significantly overestimates the reaction cross sections of the titled reaction system.

IIIh. Branching Ratios. Table 1 lists detailed product branching ratios (BR's) for the V⁺ + H₂O reaction with V⁺ prepared in single spin-orbit coupled J states obtained in the $E_{\rm cm}$ range from 0.1 to 10.0 eV. For the V⁺(a⁵D₀) + H₂O reaction in the $E_{\rm cm}$ range 0.1–1.0 eV, only the $\sigma({\rm VO}^+)$ for the formation of VO+ product ion can be observed, and thus BR(VO⁺) has a value of unity. As E_{cm} increases from 1.0 to 4.0 eV, BR(VO⁺) gradualy drecreases from 1.00 to 0.36 due to the appearances of product VH+ and VOH+ ions, which start to form near $E_{\rm cm}$ = 1.0 and 3.0 eV, respectively. At $E_{\rm cm}$ = 4.0 eV, the BR(VO⁺), BR(VH⁺), and BR(VOH⁺) are similar to values of 0.36, 0.33, and 0.31, respectively. From $E_{cm} = 4.0$ to 6.0 eV, BR(VO⁺) shows a bump with peak value of 0.45 at 6.0 eV, BR(VH⁺) continues to increase from 0.33 to 0.51, and BR(VOH+) decreases to 0.04. This observation is consistent with the corresponding σ changes. In the E_{cm} range 6.0–10.0 eV, BR(VOH⁺) has a value of 0.00 since no VOH⁺ product ion is detected. The VH+ product ion becomes the dominant product ion species at $E_{\rm cm} > 6.0$ eV.

For the V⁺(a⁵F₁) + H₂O reaction, VO⁺ is the only reaction product ion observed in the $E_{\rm cm}$ range of 0.1–0.3 eV. As $E_{\rm cm}$ is increased from $E_{\rm cm}$ = 0.3 to 3.0 eV, BR(VO⁺) monotonically decreases from 1.00 to 0.00 and BR(VOH⁺) increases from 0.00 to 0.92. The product VH⁺ ion starts to show up near $E_{\rm cm}$ = 2.5 eV. From $E_{\rm cm}$ = 3.0 to 7.0 eV, BR(VO⁺) increases continuously from 0.00 to 0.80, BR(VH⁺) exhibits a bump with the peak value of 0.11 near $E_{\rm cm}$ = 4.0 eV, and BR(VOH⁺) decreases from 0.92 to 0.09. As $E_{\rm cm}$ is increased from 7.0 to 10.0 eV, the product VOH⁺ ion disappears, and the donimant product ion species switches from VO⁺ to VH⁺.

Different from V⁺(a⁵D₀) + H₂O and V⁺(a⁵F₁) + H₂O, V⁺(a³F₂) + H₂O has two product ions, VO⁺ and VOH⁺, in the range $E_{\rm cm} = 0.1-1.0$ eV. As the $E_{\rm cm}$ is increased from 0.1 to 1.0 eV, the dominant product ion is switched from VO⁺ to VOH⁺: BR(VO⁺) gradually decreases from 0.79 at $E_{\rm cm} = 0.1$ eV to 0.39 at $E_{\rm cm} = 1.0$ eV, and in constrast, BR(VOH⁺) increases from 0.21 at $E_{\rm cm} = 0.1$ eV to 0.61 at $E_{\rm cm} = 1.0$ eV. At $E_{\rm cm} = 1.0-3.0$ eV, the VH⁺ product ion starts to be formed, BR(VH⁺) increases quickly to 0.44 at $E_{\rm cm} = 3.0$ eV, BR(VOH⁺) continues to decrease to 0.12 at $E_{\rm cm} = 3.0$ eV, and BR(VOH⁺) is still the highest one but it drops to 0.44 at $E_{\rm cm} = 3.0$ eV. In the range $E_{\rm cm} = 3.0-10.0$ eV, the VH⁺ ion becomes the dominant product ion, BR(VO⁺) shows a small bump from $E_{\rm cm} = 4.0$ to 6.0 eV with a peak value of 0.29 at 5.0 eV, and BR(VOH⁺) further deceases to 0.03 near $E_{\rm cm} = 10.0$ eV.

On the basis of the detailed product ion measurements presented above, we can generally conclude that the dominant product ion is VO⁺, preferred to be produced at lower $E_{\rm cm}$ values (<1.0 eV), whereas the VH⁺ ion becomes the most abundant product ion at higher $E_{\rm cm}$ (>7.0 eV). The shifting of

Table 1. Branching Ratios (BR's) of VO⁺ + H₂ (Including VO⁺ + H + H at $E_{cm} > 3.5$ eV), VH⁺ + OH, and VOH⁺ + H Reaction Product Channels for the Reaction of V⁺ + H₂O with V⁺ Prepared at Each of Its Three Spin–Orbit Coupled Electronic States, a^5D_0 , a^5F_1 , and a^3F_2 in the E_{cm} Range of 0.1–10.0 eV^a

	$V^{+}(a^{5}D_{0}) + H_{2}O$			$V^{+}(a^{5}F_{1}) + H_{2}O$			$V^{+}(a^{3}F_{2}) + H_{2}O$		
$E_{\rm cm}~({\rm eV})$	BR(VO ⁺)	BR(VH ⁺)	BR(VOH+)	BR(VO+)	BR(VH ⁺)	BR(VOH+)	BR(VO ⁺)	BR(VH ⁺)	BR(VOH+)
0.1	1.00	0.00	0.00	1.00	0.00	0.00	0.79	0.00	0.21
0.2	1.00	0.00	0.00	1.00	0.00	0.00	0.75	0.00	0.25
0.3	1.00	0.00	0.00	1.00	0.00	0.00	0.67	0.00	0.33
0.4	1.00	0.00	0.00	0.95	0.00	0.05	0.64	0.00	0.36
0.5	1.00	0.00	0.00	0.94	0.00	0.06	0.59	0.00	0.41
0.6	1.00	0.00	0.00	0.90	0.00	0.10	0.53	0.00	0.47
0.7	1.00	0.00	0.00	0.90	0.00	0.10	0.49	0.00	0.51
0.8	1.00	0.00	0.00	0.85	0.00	0.15	0.45	0.00	0.55
0.9	1.00	0.00	0.00	0.82	0.00	0.18	0.39	0.00	0.61
1.0	0.99	0.00	0.01	0.78	0.00	0.22	0.39	0.00	0.61
1.5	0.94	0.00	0.06	0.72	0.00	0.28	0.28	0.01	0.72
2.0	0.84	0.00	0.16	0.63	0.00	0.38	0.20	0.05	0.75
2.5	0.63	0.00	0.37	0.47	0.04	0.49	0.13	0.22	0.65
3.0	0.49	0.09	0.42	0.00	0.08	0.92	0.12	0.44	0.44
4.0	0.36	0.33	0.31	0.32	0.11	0.57	0.23	0.55	0.22
5.0	0.43	0.39	0.17	0.60	0.06	0.34	0.29	0.58	0.12
6.0	0.45	0.51	0.04	0.80	0.05	0.15	0.20	0.74	0.06
7.0	0.36	0.64	0.00	0.80	0.10	0.09	0.10	0.87	0.02
8.0	0.31	0.69	0.00	0.62	0.38	0.00	0.03	0.94	0.03
9.0	0.35	0.65	0.00	0.52	0.48	0.00	0.01	0.96	0.03
10.0	0.24	0.76	0.00	0.42	0.58	0.00	0.02	0.95	0.03

^aThe error limits of ± 0.01 represent estimated uncertainties from run-to-run independent measrements.

the peak-value positions on $E_{\rm cm}$ mainly depends on the electronic states of the reactant V⁺ ion. The VOH⁺ ion becomes the product ion species that has the highest σ 's at $E_{\rm cm}$ = 2.0–3.0 and 0.7–2.5 eV for V⁺(a⁵F₁) + H₂O and V⁺(a³F₂) + H₂O, respectively.

Illi. E_T Threshold Energy of Reaction Approach for Bond Energy Measurements. As pointed out above in section IIId, the effect of the thermal motion of neutral gaseous H_2O molecules in the reaction cell at 298 K is expected to contribute the most significant uncertainty of collision energy in this case. Chantry has shown that the kinetic energy distribution at E_{cm} has the full-width-at-half-maximum of

$$W_{1/2} = \sqrt{[11.1 \times \gamma kT \times E_{\rm cm}]} \tag{17}$$

Here, T=298 K of neutral H_2O gas, k is the Boltzmann constant, and $\gamma=[m^+/(M+m^+)]$, where m^+ and M are the masses of reactant ion and reactant neutral, respectively. For the reaction of $V^+ + H_2O$, $m^+=51$ amu, M=18 amu, and $\gamma=51/69$. Due to the Doppler broadening effect from H_2O thermal kinetic motion, the E_T value should be downshifted from the true onset of reaction E_0 . At $E_{\rm cm}=E_0$ (the true reaction onset) the kinetic energy spread is $W_{1/2}=2\Delta E=\sqrt{[11.1\times \gamma kT\times E_0]}=\sqrt{[0.211\times E_0]}$. Assuming the E_T onset is observed when H_2O moves against V^+ with a kinetic energy lower by the half-maximum of the distribution, we then have $E_0=E_T+\Delta E$. This yields eqs 18 and 19, which allow the calculation of ΔE from E_T .

$$W_{1/2} = \sqrt{[0.211 \times E_0]}$$

= $\sqrt{[0.211 \times (E_T + \Delta E)]}$
= $2\Delta E$ (18)

$$4\Delta E^2 - 0.211\Delta E - (0.211E_{\rm T}) = 0 \tag{19}$$

As discussed in section IIId, on the basis of the measured $E_{\rm T}$ thresholds for the $\sigma(a^5D_i: VH^+)$, $\sigma(a^5F_i: VH^+)$, and $\sigma(a^3F_i: VH^+)$ VH⁺), we have deduced an upper bound value of 2.6 ± 0.2 eV for the $D_0(V^+-H)$. Similarly, the measured E_T thresholds for the $\sigma(a^5D_i: VOH^+)$ and $\sigma(a^5F_i: VOH^+)$ have yielded the determination of an upper limit of $D_0(V^+-OH) = 4.3 \pm 0.3$ eV. After taking into account and correcting for the ΔE term deduced from eqs 17-19 resulting from the Doppler broadening effect of the H₂O molecule, we have obtained the $D_0(V^+-H) = 2.2 \pm 0.2$ eV and $D_0(V^+-OH) = 4.0 \pm 0.3$ eV by using eqs 13 and 14, respectively. These D_0 values obtained in the present study on the basis of E_T threshold energy measurements are in agreement with the results $[D_0(V^+-H) = 2.02 \pm 0.05 \text{ eV} \text{ and } D_0(V^+-OH) = 4.41 \pm$ 0.19 eV] reported previously on the basis of the simulation approach. Since the simulation approach is recognized to be the more precise method for D_0 measurements, this agreement observed also indicates that the $E_{\rm T}$ threshold energy measurement scheme can also be employed as a reliable method for the determination of bond dissociation energies of TM-containing product ions involved.

The $E_{\rm T}$ threshold detection method presented here has the advantage of being straightforward with tractable physical insight. When combined with high-level ab initio quantum-chemical calculations, both the $E_{\rm T}$ threshold and the simulation approaches can be profitable for the study of energetics and bonding properties of TM-ligated chemical species, many of which are still unavailable in the literature. Although the present experiment reported here does not involve any high resolution energetic studies, we have demonstrated that the ease of producing exotic TM-containing transient species for experimentation make it highly attractive

as a technique for guiding theoretical studies on chemical structure and chemical reactivity, particularly involving bonding properties between TM cations and ligands.

IV. CONCLUSION AND SUMMARY

In this work, we report on a detailed investigation of the σ values of the quantum-electronic-state-selected ion-molecule reaction of V+ + H2O, in which the TM V+ reactant cation is prepared in single quantum spin-orbit coupled J states, a⁵D_{0.2}, $a^5F_{1,2}$, and $a^3F_{2,3}$ in the E_{cm} range from 0.1 to 10.0 eV. The effects of the quantum-electronic state of V^+ and E_{cm} on the chemical reactivity have been examined. Three product channels VO⁺ + H₂, VH⁺ + OH, and VOH⁺ + H of the V⁺ + H₂O reaction are unambiguously identified on the basis of the E_{cm} threshold and electronic-state-selected $\sigma(a^5D_{0.2}, a^5F_{1.2}, a^5F_{1.2$ and $a^3F_{2,3}$) curve measurements. These E_T thresholds measured for the σ curves also allow the determination of upper bound 0 K bond dissociation energies for $D_0(V^+-H) =$ $2.6 \pm 0.2 \text{ eV}$ and $D_0(V^+-OH) = 4.3 \pm 0.3 \text{ eV}$. The chemical reactivity of the titled reaction system is found to be dominantly governed by the conservation of total electron spins where the triplet states, a³F_{2,3}, of V⁺ exhibit much higher reactivity toward the water molecule than those of the two quintet a⁵D_{0.2} and a⁵F_{1.2} electronic states. This experimental observation is consistent with the results of the $V^+ + D_2$ (CO₂, CH₄) reactions, ^{9,10} showing that a "weak quintet-to-triplet spin crossing" mechanism is operative. No J-state dependences are observed for this titled reaction system. In addition, detailed branching ratios of product ions as a function of both quantum-electronic states and $E_{\rm cm}$ have also been determined. The large differences between σ values for different V⁺ electronic states reported in this work, can be used for effective control of H₂ production by quantum-electronic-state selection.

AUTHOR INFORMATION

Corresponding Author

Cheuk-Yiu Ng — Department of Chemistry, University of California, Davis, California 95616, United States;
occid.org/0000-0003-4425-5307; Email: cyng@ucdavis.edu

Authors

Yuntao Xu — Department of Chemistry, University of California, Davis, California 95616, United States; ⊚ orcid.org/0000-0002-1205-8168

Yih-Chung Chang — Department of Chemistry, University of California, Davis, California 95616, United States

Matthew Parziale – Department of Chemistry, University of California, Davis, California 95616, United States

Anna Wannenmacher – Department of Chemistry, University of California, Davis, California 95616, United States

Complete contact information is available at: https://pubs.acs.org/10.1021/acs.jpca.0c07884

Notes

The authors declare no competing financial interest.

ACKNOWLEDGMENTS

This work is supported by the National Science Foundation under CHE-1763319. C.Y.N. is also grateful to Dr. Huie Tarng Liou for his generous donation of research support for the Ng

Laboratory. Mr. Jie Wang also acknowledges the support of a visiting student Fellowship by the Physics Department of Tsinghua University, Beijing, China.

REFERENCES

- (1) Burgess, J. Metal ions in solution; Ellis Horwood, 1978.
- (2) Marcus, Y. Ions in Solution and Their Solvation; Wiley, 2015.
- (3) Ni, M.; Leung, M. K. H.; Leung, D. Y. C.; Sumathy, K. A review and recent developments in photocatalytic water-splitting using TiO2 for hydrogen production. *Renewable Sustainable Energy Rev.* **2007**, *11* (3), 401–425.
- (4) Armentrout, P. B.; Beauchamp, J. L. The chemistry of atomic transition-metal ions: insight into fundamental aspects of organometallic chemistry. *Acc. Chem. Res.* **1989**, 22 (9), 315–321.
- (5) Böhme, D. K.; Schwarz, H. Gas-phase catalysis by atomic and cluster metal ions: The ultimate single-site catalysts. *Angew. Chem., Int. Ed.* **2005**, 44 (16), 2336–2354.
- (6) Condon, E. U.; Condon, E. U.; Shortley, G. H. The Theory of Atomic Spectra; Cambridge University Press, 1951.
- (7) Elkind, J. L.; Armentrout, P. B. Effect of kinetic and electronic energy on the reaction of V⁺ with molecular hydrogen, hydrogen deuteride, and molecular deuterium. *J. Phys. Chem.* **1985**, 89 (26), 5626–5636.
- (8) Koyanagi, G. K.; Bohme, D. K. Gas-phase reactions of carbon dioxide with atomic transition-metal and main-group cations: room-temperature kinetics and periodicities in reactivity. *J. Phys. Chem. A* **2006**, *110* (4), 1232–1241.
- (9) Xu, Y.; Chang, Y.-C.; Ng, C.-Y. Chemical Activation of a Deuterium Molecule by Collision with a Quantum Electronic State-Selected Vanadium Cation. *J. Phys. Chem. A* **2019**, *123* (28), 5937–5944.
- (10) Chang, Y. C.; Xu, Y.; Ng, C.-Y. Quantum state control on the chemical reactivity of a transition metal vanadium cation in carbon dioxide activation. *Phys. Chem. Chem. Phys.* **2019**, 21 (13), 6868–6877.
- (11) Armentrout, P. Electronic state-specific transition metal ion chemistry. *Annu. Rev. Phys. Chem.* **1990**, 41 (1), 313–344.
- (12) Weisshaar, J. C., Control of Transition-Metal Cation Reactivity by Electronic State Selection. In *Advances in Chemical Physics: State-Selected and State-To-State Ion—Molecule Reaction Dynamics, Part 1. Experiment*; Ng, C. Y.; Baer, M., Eds.; John Wiley & Sons, Inc., 1992; Vol. 82, pp 213–262.
- (13) Schröder, D.; Shaik, S.; Schwarz, H. Two-state reactivity as a new concept in organometallic chemistry. *Acc. Chem. Res.* **2000**, 33 (3), 139–145.
- (14) Ng, C. Y. State-selected and state-to-state ion-molecule reaction dynamics. J. Phys. Chem. A 2002, 106 (25), 5953-5966.
- (15) Ng, C. Y.; Baer, M. State selected and state to state ion molecule reaction dynamics, Part 1: Experiment; John Wiley & Sons, Inc., 1992; Vol. 82
- (16) Xu, Y.; Xiong, B.; Chang, Y. C.; Ng, C. Y. Quantum-vibrational-state-selected integral cross sections and product branching ratios for the ion–molecule reactions of $N_2^+(X^2\Sigma_g^+; \nu^+=0-2)+H_2O$ and $H_2O^+(X^2B_1: \nu_1^+\nu_2^+\nu_3^+=000$ and $100)+N_2$ in the collision energy range of 0.04–10.00 eV. Astrophysical Journal **2018**, 861 (1), 17.
- (17) Xu, Y.; Xiong, B.; Chang, Y. C.; Pan, Y.; Lo, P. K.; Lau, K. C.; Ng, C. Y. A quantum-rovibrational-state-selected study of the $H_2O^+(X^2B_1:\nu_1^+\nu_2^+\nu_3^+;\ N^+K_a^+K_b^+)$ + CO reaction in the collision energy range of 0.05–10.00 eV: translational, rotational, and vibrational energy effects. *Phys. Chem. Chem. Phys.* **2017**, *19* (15), 9778–9789.
- (18) Xiong, B.; Chang, Y. C.; Ng, C. Y. A quantum-rovibrational-state-selected study of the proton-transfer reaction ${\rm H_2}^+(X^2\Sigma_{\rm g}^+\colon \nu^+=1-3;\ N^+=0-3)$ + Ne \to NeH⁺+ H using the pulsed field ionization-photoion method: observation of the rotational effect near the reaction threshold. *Phys. Chem. Chem. Phys.* **2017**, *19* (28), 18619–18627.

- (19) Xu, Y.; Xiong, B.; Chang, Y. C.; Ng, C. Y. The translational, rotational, and vibrational energy effects on the chemical reactivity of water cation $H_2O^+(X^2B_1)$ in the collision with deuterium molecule D_2 . J. Chem. Phys. **2013**, 139 (2), 024203.
- (20) Xiong, B.; Chang, Y.-C.; Ng, C.-Y. Quantum-state-selected integral cross sections for the charge transfer collision of $O_2^+(a\ ^4\Pi_{u\ 5/2,\ 3/2,\ 1/2,\ 1/2}:v^+=1-2;\ J^+)$ [$O_2^+(X^2\Pi_{g\ 3/2,\ 1/2}:v^+=22-23;\ J^+)$]+ Ar at center-of-mass collision energies of 0.05–10.00 eV. *Phys. Chem. Chem. Phys.* **2017**, *19* (43), 29057–29067.
- (21) Polanyi, J. C. Concepts in reaction dynamics. Acc. Chem. Res. **1972**, 5 (5), 161–168.
- (22) Gruebele, M.; Wolynes, P. G. Vibrational Energy Flow and Chemical Reactions. Acc. Chem. Res. 2004, 37 (4), 261–267.
- (23) Crim, F. F. Chemical dynamics of vibrationally excited molecules: Controlling reactions in gases and on surfaces. *Proc. Natl. Acad. Sci. U. S. A.* **2008**, *105* (35), 12654–12661.
- (24) Liu, K. Vibrational Control of Bimolecular Reactions with Methane by Mode, Bond, and Stereo Selectivity. *Annu. Rev. Phys. Chem.* **2016**, 67 (1), 91–111.
- (25) Reiher, M. A theoretical challenge: Transition-metal compounds. *Chimia* **2009**, *63* (3), 140–145.
- (26) Veillard, A. Quantum Chemistry: The Challenge of Transition Metals and Coordination Chemistry; Springer: Netherlands, 2012.
- (27) Clemmer, D.; Chen, Y.-M.; Aristov, N.; Armentrout, P. Kinetic and Electronic Energy Dependence of the Reaction of V+ with D2O. *J. Phys. Chem.* **1994**, *98* (31), 7538–7544.
- (28) Irigoras, A.; Fowler, J. E.; Ugalde, J. M. Reactivity of Sc⁺ (³D, ¹D) and V⁺ (⁵D, ³F): Reaction of Sc⁺ and V⁺ with Water. *J. Am. Chem. Soc.* **1999**, *121* (3), 574–580.
- (29) Koyanagi, G. K.; Bohme, D. K.; Kretzschmar, I.; Schröder, D.; Schwarz, H. Gas-phase chemistry of bare V⁺ cation with oxygen and water at room temperature: Formation and hydration of vanadium oxide cations. *J. Phys. Chem. A* **2001**, *105* (17), 4259–4271.
- (30) Marinelli, P. J.; Squires, R. R. Sequential solvation of atomic transition-metal ions. The second solvent molecule can bind more strongly than the first. *I. Am. Chem. Soc.* **1989**, *111* (11), 4101–4103.
- (31) Chang, Y. C.; Xiong, B.; Xu, Y.; Ng, C.-Y. Quantum Spin—Orbit Electronic State Selection of Atomic Transition Metal Vanadium Cation for Chemical Reactivity Studies. *J. Phys. Chem. A* **2019**, *123* (12), 2310–2319.
- (32) Balat, M. Potential importance of hydrogen as a future solution to environmental and transportation problems. *Int. J. Hydrogen Energy* **2008**, 33 (15), 4013–4029.
- (33) Wang, M.; Wang, Z.; Gong, X.; Guo, Z. The intensification technologies to water electrolysis for hydrogen production—A review. *Renewable Sustainable Energy Rev.* **2014**, *29*, 573—588.
- (34) Li, D.; Shi, J.; Li, C. Transition-Metal-Based Electrocatalysts as Cocatalysts for Photoelectrochemical Water Splitting: A Mini Review. *Small* **2018**, *14* (23), 1704179.
- (35) Chang, Y. C.; Xu, Y.; Lu, Z.; Xu, H.; Ng, C. Rovibrationally selected ion—molecule collision study using the molecular beam vacuum ultraviolet laser pulsed field ionization-photoion method: Charge transfer reaction of N_2^+ ($X^2\Sigma_g^+$; v^+ = 0–2; N^+ = 0–9)+ Ar. *J. Chem. Phys.* **2012**, 137 (10), 104202.
- (36) Chantry, P. J. Doppler broadening in beam experiments. *J. Chem. Phys.* **1971**, 55 (6), 2746–2759.
- (37) Chang, Y. C.; Xu, Y.; Xiong, B.; Ng, C.-Y. Chemical activation of oxygen molecule by quantum electronic state selected vanadium cation: observation of spin—orbit state effects. *Mol. Phys.* **2020**, 1–11.
- (38) Friedlander, G.; Kennedy, J. W.; Macias, E. S. Nuclear and Radiochemistry; Wiley, 1981.
- (39) Chase, M. W., Jr. NIST-JANAF thermochemical tables. J. Phys. Chem. Ref. Data, Monograph 1998, 9.
- (40) Ruscic, B.; Pinzon, R. E; Laszewski, G. v.; Kodeboyina, D.; Burcat, A.; Leahy, D.; Montoy, D.; Wagner, A. F Active thermochemical tables: thermochemistry for the 21st century. *J. Phys.: Conf. Ser.* **2005**, *16* (1), 561.

- (41) Dyke, J. M.; Gravenor, B. W. J.; Hastings, M. P.; Morris, A. High-temperature photoelectron spectroscopy: the vanadium monoxide molecule. *J. Phys. Chem.* **1985**, 89 (21), 4613–4617.
- (42) Luo, Z.; Chang, Y. C.; Lam, C. S.; Lau, K. C.; Ng, C. Y. Chapter 6 Two-Color Pulsed-Field Ionization-Photoelectron Spectroscopy: A Quest to Benchmark State-of-the-Art ab initio Quantum Electronic Structure Calculations of Spectroscopic and Energetic Properties for Transition Metal-Containing Species. In *Frontiers and Advances in Molecular Spectroscopy*; Laane, J., Ed.; Elsevier, 2018; pp 195–249.
- (43) Sievers, M.; Armentrout, P. B. Potential energy surface for carbon-dioxide activation by V^+ : A guided ion beam study. *J. Chem. Phys.* **1995**, 102 (2), 754–762.
- (44) Lessen, D. E.; Asher, R. L.; Brucat, P. J. Vibrational structure of an electrostatically bound ion—water complex. *J. Chem. Phys.* **1990**, 93 (8), 6102–6103.
- (45) Walker, N.; Walters, R.; Pillai, E.; Duncan, M. Infrared spectroscopy of $V^+(H_2O)$ and $V^+(D_2O)$ complexes: Solvent deformation and an incipient reaction. *J. Chem. Phys.* **2003**, *119* (20), 10471–10474.
- (46) Gioumousis, G.; Stevenson, D. Reactions of gaseous molecule ions with gaseous molecules. V. Theory. *J. Chem. Phys.* **1958**, 29 (2), 294–299.
- (47) Su, T.; Bowers, M. T. Ion-Polar molecule collisions: the effect of ion size on ion-polar molecule rate constants; the parameterization of the average-dipole-orientation theory. *Int. J. Mass Spectrom. Ion Phys.* **1973**, *12* (4), 347–356.
- (48) Schwarz, H. On the spin-forbiddeness of gas-phase ion—molecule reactions: a fruitful intersection of experimental and computational studies. *Int. J. Mass Spectrom.* **2004**, 237 (1), 75–105.